Synthesis and characterization of an extended tetrathiafulvalene derivative coordinated to copper iodide and its charge-transfer and radical ion salts

J. Ramos,[a] V. M. Yartsev,[a,b] S. Golhen,[c] L. Ouahab[c] and P. Delhaès[a]*

[a]*Centre de Recherche Paul Pascal, CNRS et Universite Bordeaux I, Av. Albert Schweitzer, 33600 Pessac, France*
[b]*Centro de Fisica, IVIC, Apartado 21827, Caracas 1020-A, Venezuela*
[c]*Laboratoire de Chimie du Solide et Inorganique Moleculaire, URA 1495 CNRS, Universite de Rennes I, 35042 Rennes Cedex, France*

A new bisfunctional TTF type donor molecule (D–σ–D) with a copper iodine bridge has been synthesized and characterized. Its salts have been prepared using standard crystallization techniques. The structural, electrical, optical and low-temperature magnetic properties of these new compounds have been investigated. It has been shown in particular that the compound (D–σ–D)$(TCNQ)_3$ presents a low-temperature magnetic ground state which is connected to the antiferromagnetic interactions of the bis-radical cation. This result opens the way to prepare new extended-hybrid TTF molecules containing paramagnetic metals showing related magnetic and electrical properties.

Intensive work on extended tetrathiafulvalene (TTF) type donors in recent years (see ref. 1 and 2) has resulted in the synthesis of conducting salts with 1:1 stoichiometry. This is the most obvious consequence of an increased molecular size and a corresponding decrease of the Coulomb correlation energy between two electrons occupying the same MO with opposite spins. Extended π-electron conjugated bis-fused[3] and tris-fused[4] tetrathiafulvalenes as well as non-conjugated systems (D–σ–D type) are found to exist; both types of system are potential donors for organic conductors and ferromagnets as well as being multiredox systems.[1] In radical ion salts, extended donors usually form segregated stacks along one crystallographic axis but the presence of many side-by-side short S···S contacts leads to the formation of conducting two-dimensional sheets even if some compounds present alternate stacks.[5] Spectroscopic[6,7] and magnetic[8] studies provide useful information about electronic correlations and also electron–molecular vibration (EMV) coupling revealed by the appearance of so-called vibronic modes: these effects are especially influenced by a modification of the molecular size. The decrease of the Coulomb repulsion energy in extended ions results in a shift of the charge-transfer band to lower energy and more effective coupling between π electrons and intramolecular vibrations.

A complementary approach[9,10] is based on the idea of introducing transition metals connected with TTF derivatives as for example in copper iodide coordination polymers. In such a hybrid compound, it is also possible to tune the valence state of the introduced metal for intervalence electronic transitions.[11,12] Following this track we have been interested in the synthesis of bis(ethylenedithiodimethylthiotetrathiafulvalene copper iodide) **2**, the extended donor obtained by connecting two BEDT analogues (ethylenedithiodimethylthiotetrathiafulvalene, EDT-DMT-TTF, **1**) by a Cu–I_2–Cu bridge (D–σ–D type) (Fig. 1). This compound represents an improvement over similar polymeric complexes already described[10] since it is soluble and has allowed us to prepare crystalline radical ion salts as **2**(BF_4) and charge-transfer salts such as **2**$(TCNQ)_3$.

Here, we report the synthesis, chemical characterization and crystal structure of the new hybrid π donor molecule **2**. We study the spectroscopic, electric and low-temperature magnetic properties of the obtained charge-transfer and radical ion salts, and finally we propose some explanations and correlation between them.

Chemical preparation and structural characterization

Synthesis of products

To prepare the unsymmetrical compound **1**, the first step is the synthesis of the precursor thiones following a known method.[13] Then one has to couple them through the usual procedure with trimethylphosphite, followed by chromatography on a silica gel column to separate the symmetrical and unsymmetrical products. Compound **1** (unsymmetrical) is obtained in a total yield of *ca.* 5%.

In the next step **1** is dissolved in dry warm acetonitrile, then mixed with a stoichiometric amount of copper(I) iodide in the same solvent. The complex precipitated immediately but the mixture is left overnight to complete the process. The final product **2** was recrystallized in acetonitrile and orange single crystals were obtained in a yield of 80%.

The mass spectrometry (FAB technique) has evidenced both the presence of copper and the organic ligands. The elemental analysis (found: C, 21.11; H, 1.37; I, 21.78; Cu, 10.92; S, 44.38%. Calc.: C, 20.81; H, 1.75; I, 21.99; Cu, 11.01; S, 44.44%) confirms the proposed structure. This compound shows no EPR signal, indicating the presence of Cu^I and that **2** is diamagnetic.

X-Ray crystal structure

The crystal data for a single crystal has been obtained on an Enraf-Nonius CAD4 diffractometer. The crystal acquisition data are summarized in Table 1 and the crystal structure is

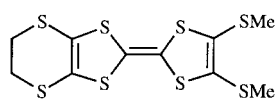

1

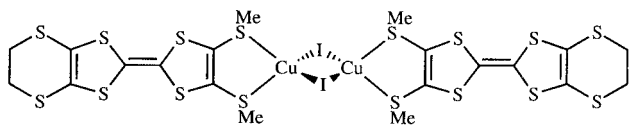

2

Fig. 1 Unsymmetrical ligand **1** and complex **2**

Table 1 Crystal data and refinement for compound **2**

formula	$C_{20}H_{20}Cu_2I_2S_{16}$
formula mass	1154.20
crystal system	monoclinic
space group	*C*2
a/Å	25.326(13)
b/Å	8.7161(11)
c/Å	34.868(13)
β/degrees	111.30(2)
V/Å^3	7171(5)
Z	8
D_c/g cm^{-3}	2.138
crystal dimensions/mm	0.5 × 0.1 × 0.1
radiation (*λ*/Å)	Mo-K*α*(0.710 73)
temperature	293 K
scan method	*θ*–2*θ*
θ range/degrees	1.25–25.97
range of *hkl*	−31/28, 0/10, 0/42
μ(Mo-K*α*)/mm^{-1}	3.857
collected reflections	7496
independent reflections (R_{int})	7374(0.0335)
absorption correction	*ψ*-scan
transmission (max., min.)	0.999, 0.91
R indices [$I > 2\sigma(I)$]	$R_1 = 0.0575$, $wR_2 = 0.1698$
S, on F^2	1.188
$\Delta\rho$/e Å^{-3} (max., min.)	1.167, −1.233

shown in Fig. 2. Selected bond distances and angles including those of the copper–iodine–copper bridge between the two donor molecules are listed in Table 2.†

The unit cell is based on two independent molecules A and B forming dimers as shown in Fig. 2 with slightly different

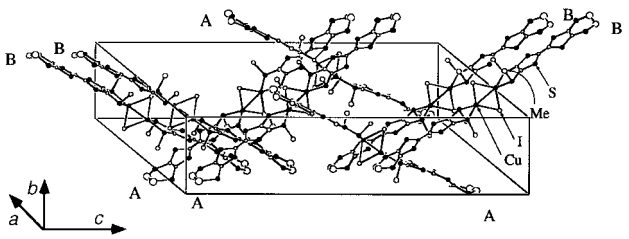

Fig. 2 X-Ray structure of a (D–*σ*–D) molecular crystal

Table 2 Selected bond distances (Å) and bond angles (degrees) with standard deviations in parentheses

Cu(1)—S(2)	2.398(8)	Cu(3)—S(18)	2.392(8)
Cu(1)—S(1)	2.430(8)	Cu(3)—S(17)	2.408(8)
Cu(1)—I(2)	2.571(4)	Cu(3)—I(4)	2.576(4)
Cu(1)—I(1)	2.626(4)	Cu(3)—I(3)	2.625(4)
Cu(2)—S(9)	2.351(8)	Cu(3)—Cu(4)	2.734(5)
Cu(2)—S(10)	2.371(8)	Cu(4)—S(26)	2.351(8)
Cu(2)—I(1)	2.586(4)	Cu(4)—S(25)	2.360(8)
Cu(2)—I(2)	2.635(4)	Cu(4)—I(3)	2.590(4)
Cu(1)—Cu(2)	2.732(5)	Cu(4)—I(4)	2.633(4)
S(2)—Cu(1)—S(1)	88.1(3)	S(18)—Cu(3)—S(17)	88.7(3)
S(9)—Cu(2)—S(10)	90.7(3)	S(26)—Cu(4)—S(25)	91.3(3)
I(2)—Cu(1)—I(1)	117.1(2)	I(4)—Cu(3)—I(3)	117.1(2)
I(1)—Cu(2)—I(2)	116.2(2)	I(3)—Cu(4)—I(4)	116.28(14)
S(2)—Cu(1)—I(2)	115.6(2)	S(18)—Cu(3)—I(4)	115.3(2)
S(1)—Cu(1)—I(2)	109.5(2)	S(17)—Cu(3)—I(4)	109.3(2)
S(2)—Cu(1)—I(1)	110.4(2)	S(18)—Cu(3)—I(3)	110.2(2)
S(1)—Cu(1)—I(1)	112.7(2)	S(17)—Cu(3)—I(3)	112.9(2)
S(9)—Cu(2)—I(1)	115.5(2)	S(26)—Cu(4)—I(3)	115.0(2)
S(10)—Cu(2)—I(1)	114.5(2)	S(25)—Cu(4)—I(3)	113.7(2)
S(9)—Cu(2)—I(2)	109.5(2)	S(26)—Cu(4)—I(4)	110.1(2)
S(10)—Cu(2)—I(2)	107.5(2)	S(25)—Cu(4)—I(4)	107.6(2)

† Atomic coordinates, thermal parameters, and bond lengths and angles have been deposited at the Cambridge Crystallographic Data Centre (CCDC). See Information for Authors, *J. Mater. Chem.*, 1997, Issue 1. Any request to the CCDC for this material should quote the full literature citation and the reference number 1145/38.

bond lengths, comparable with those determined in previous work on a similar molecule.[10] The most striking feature is the coplanarity of both donor molecules, symmetrically with respect to the central bridging iodine atoms. The equivalence of both donor units, coupled with the long bridging element, will affect the properties of **2**, which behaves in some respects as two isolated molecules of **1**.

Radical ion salts

We have carried out cyclic voltammetry on **2** under standard conditions, in acetonitrile containing 0.1 M $NBu^n_4PF_6$ employing a glassy carbon working electrode, a Ag/AgCl reference electrode and a Pt counter electrode, sweeping between −1.5 and +1.2 V at a rate of 100 mV s^{-1}.

Two reversible oxidation waves are detected, with $E_{\frac{1}{2}}$ values of 0.51 and 0.77 V. A reduction wave is found at −0.78 V which is not reversible owing to some chemical reaction. From these results we attribute the two oxidation waves to the formation of bis-monocationic and bis-dicationic species; indeed these values are quite similar to those already found in BEDT-TTF.[14] The reduction wave could be due to the reduction of Cu^I to Cu^0 which causes decomposition of the complex. It is interesting that we do not observe any oxidation wave of Cu^I to Cu^{II} between 0.5 and 1.5 V as might be expected for an intervalence charge transfer.

We have also prepared salts of **2** by electro-oxidation and direct oxidation in the liquid phase. In the first case we used a classical two-compartment electrochemical cell with Pt electrodes under usual conditions (0.1 M $NBu^n_4BF_4$ or $NBu^n_4PF_6$ in dry CH_3CN under an electric current of 1 μA) and obtained black–green single-crystal needles of **2**(BF_4) and **2**(PF_6).

In the second method we used a U-shaped diffusion cell in which **2** and neutral TCNQ are stored in different compartments ($c \approx 10^{-3}$ M). When equimolecular quantities were used there remained an excess of the neutral molecule **2**. After three or four weeks we obtained black crystalline fibres of **2**$(TCNQ)_n$ (with $TCNQF_4$ a blue–black powder was obtained).

Crystal structure and stoichiometry of the charge-transfer salts

The quality of the single-crystals of both compounds allowed us only to obtain the unit-cell parameters. For the BF_4 salt, using an Enraf-Nonius CAD4 diffractometer, we found a monoclinic structure (*P*2/*c*) with the following parameters: *a* = (3.75 Å)*n*, *b* = 22.62 Å, *c* = 11.60 Å, *β* = 97.60°; the crystal structure of the PF_6 salt is isomorphous.

Because the TCNQ charge-transfer compound showed many defects, only the Laue photographic technique was employed. This compound crystallizes in the triclinic (*P*1 or *P*$\bar{1}$) system with proposed parameters *a* ≥ 20 Å, *b* ≥ 14.8 Å, *c* = 4.03 Å, *γ* = 80° and *V* ≥ 1211 Å^3 (*Z* = 1).

In both compounds we observe one large unit-cell length as found in the neutral compound (Fig. 1) which indicates the probable location of the long axis of the extended TTF molecule.

After experimental measurements of the powder density and electronic microprobe analysis (which confirmed the presence of N, S, Cu and I) it turns out that the stoichiometries are 1 : 1 for the BF_4 salt and 1 : 3 or possibly 1 : 2 for the TCNQ compound. The formulation **2**$(TCNQ)_3$ is proposed to explain the magnetic properties discussed below.

Results and discussion of physical properties

Dc conductivity measurements

The dc conductivity has been determined on single crystals using a standard four-probe method with Pt paste. The BF_4 and PF_6 salts show semiconducting behaviour with a room-temperature absolute conductivity $\sigma_{290} \approx 10^{-4}$–$10^{-5}$ S cm^{-1}

and an activation energy $E_a \approx 0.1$ eV just below 290 K. The TCNQ charge-transfer salt is much more conducting and the room-temperature dc conductivity value $\sigma \approx 0.2$ S cm^{-1} is almost constant down to 250 K. Below this temperature a progressive semiconducting regime is observed and an insulating phase is observed down to 50 K (Fig. 3). We propose the presence of a metal–insulator transition ($T_{MI} \approx$ K) as observed in similar compounds.[15]

Optical properties

VIS–IR spectra (15 000–400 cm^{-1}) have been measured at room temperature with a Nicolet 750 instrument for absorption measurements on compressed KBr pellets and with a Nicolet 740 instrument (6000–400 cm^{-1}) equipped with a Nic-Plan microscope and a SeZn polarizer for reflectivity experiments on single crystals (ϕ_{irr} *ca.* 100 μm).

In a preliminary experiment the reflectance spectra were measured from the naturally grown surface of the crystal of a neutral molecule **2** and it appears to be practically independent of the polarization. The major absorption bands are reported in Table 3 with their assignments.We associate the scale shaped surface and the observed in-plane isotropy with a two-dimensional organization in agreement with the crystal structure (Fig. 2).

The absorption spectra of KBr pellets of **2**(BF_4) and **2**(PF_6) (Fig. 4) are dominated by a broad charge-transfer band with a first maximum about 1800 cm^{-1}, a weak peak around 6000 cm^{-1} and another peak at 10 500 cm^{-1}. The reflectance, measured parallel to the needle axis [Fig. 5(a)] shows a strong dispersion below 4000 cm^{-1} attributable to a charge-transfer excitation involving the extended π donor system. In the polarization perpendicular to the needle axis [Fig. 5(b)], we observe at the same wavenumber a much less pronounced feature which could be associated with a charge transfer along the long molecular axis of **2**. In the simple salt of a giant derivative of TTF: $D_1(ClO_4)$ (D_1 consists of a dihydro-TTF core with two conjugated 1,4-dithiafulvalen-6-yl side-arms) the CT band is at 5600 cm^{-1}. In our case, there is no conjugation between D fragments of the D–σ–D molecule and in a simple salt of D–σ–D with BF_4 or PF_6 the hole is localized on one of the fragments D. Therefore, we ascribe the charge-transfer band in the case of parallel polarization to transitions shown by arrows in the following scheme, even if intramolecular charge transfer cannot be excluded.

$$\begin{array}{ccc} D^0\text{–}\sigma\text{–}D^+ \\ \Downarrow \quad\quad \Downarrow \\ D^+\text{–}\sigma\text{–}D^0 \end{array}$$

Following this scheme, two absorption bands at wavenumbers of 6000 and 10 500 are intermolecular charge-transfer processes arising from other combinations of charge distribution in neighbouring $(D\text{–}\sigma\text{–}D)^+$, considering each EDT–DMT–TTF (D) as an individual molecule. The low energy charge-transfer band is strongly coupled to the intermolecular vibrations (see band attribution in Table 3) and in order to explain the experimental results we use a standard molecular dimer model as in the case of complex TCNQ salts.[16] The associated complex conductivity has the form:

$$\sigma(\omega) = i\omega \frac{e^2R^2}{4V}\left(\frac{1}{\chi(\omega)} - \sum_{\alpha} \frac{g_\alpha{}^2\omega_\alpha}{\omega_\alpha{}^2 - \omega^2 - i\omega\gamma_\alpha}\right)^{-1} \quad (1)$$

where V is the volume per molecule, R denotes the distance between neighbouring molecules and the electronic polarizability is

$$\chi(\omega) = \frac{2M^2\omega_{CT}}{\omega_{CT}{}^2 - \omega^2 - i\omega\Gamma} \quad (2)$$

In eqn. (1), ω_α, g_α and γ_α are, respectively, the wavenumber, the EMV (electron–molecular vibration) coupling constant and the damping factor for the αth totally symmetric mode of intramolecular vibration. In eqn. (2), Γ is the phenomenological natural width of the originally uncoupled charge-transfer excitation with energy ω_{CT} and M is the matrix element for the charge-transfer transition. The fitting procedure which reproduces the reflectance spectrum [Fig. 5(a)] has as parameters $\omega_{CT} = 1700$ cm^{-1}, $\Gamma = 1500$ cm^{-1}, $M = 1$, $R = 4.4$ A, $V = 708$ A^3, $e_\infty = 3$ and three intramolecular vibrations at $\omega_\alpha = 1496$, 1468 and 500 cm^{-1} and $g_\alpha = 40$, 60 and 20 cm^{-1}, respectively. These parameter values correspond well to those found for similar compounds.[6]

If we compare the spectra of **2**$(TCNQ)_3$ shown in Fig. 5 and 6, with those of the simple salt of the same donor, **2**(BF_4), we observe that the charge-transfer band in the complex salt is situated at a higher wavenumber (*ca.* 3200 cm^{-1}). This means that all antiresonances in the parallel polarization [Fig. 6(a)] may be attributed to the excitation of totally symmetric intramolecular vibrations of TCNQ, which demonstrates that the charge-transfer excitation takes place along the stack composed only of the TCNQ molecules (Table 3). To a first approximation, we can assume that **2** is present as a dication and does not contribute to the charge transfer. The position of the charge-transfer band at 3200 cm^{-1} agrees well with that observed for the mixed-valence state stack of TCNQ stacks[15] and is in agreement with the relatively high dc conductivity value of the salt. The stoichiometry suggests a complete charge transfer of two electrons from **2** to a trimer of TCNQ molecules, so the appropriate model is a trimer with two radical electrons.[17] In this model there are two allowed optical transitions:

$$TCNQ^- + TCNQ^0 + TCNQ^- \rightarrow TCNQ^0 + TCNQ^- + TCNQ^-$$

$$TCNQ^- + TCNQ^- + TCNQ^0 \rightarrow TCNQ^0 + TCNQ^{2-} + TCNQ^0$$

In our case, the latter transition has much less intensity, and can be disregarded. Therefore, the expression for the complex conductivity takes the form

$$\sigma(\omega) = i\omega \frac{e^2R^2}{V}\left(\frac{\omega_{CT}{}^2 - \omega^2 - i\omega\Gamma}{2M^2\omega_{CT}} - \sum_{\alpha} \frac{g_\alpha{}^2\omega_\alpha}{\omega_\alpha{}^2 - \omega^2 - i\omega\gamma_\alpha}\right)^{-1} \quad (3)$$

where V is the volume per molecular trimer and R is the distance between neighbouring molecules. A fit of this model to the experimental data for $(D\text{–}\sigma\text{–}D)(TCNQ)_3$ is shown in Fig. 6(a). The CT excitation energy found from this fit $\omega_{CT} = 2500$ cm^{-1}, may be used to calculate the transfer integral t: $\omega_{CT} = 1.5t$ (for a typical value of $U/4t = 1$) giving $t = 0.2$ eV.

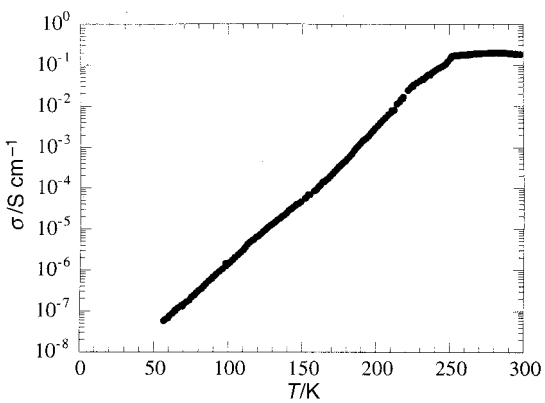

Fig. 3 Temperature dependence of the dc conductivity of a **2**$(TCNQ)_3$ single crystal measured along the long side

Table 3 IR absorption bands ($\tilde{\nu}$/cm^{-1}) for **2**, **2**(BF_4) and **2**$(TCNQ)_3$ and molecular vibration wavenumbers for bis(ethylenedithio)tetrathiafulvalene (ET) and tetracyanoquinodimethane (TCNQ) molecules and ions. Antiresonance minima are marked *

mode	ET^{0a}	ET^{+b}	**2**^{0}	**2**(BF_4)	**2**$(TCNQ)_3$	TCNQ^{0c}	TCNQ^{-d}	mode
					2223*	2225	2206	$2a_g$
					2189*			
					1596*	1600	1615	$3a_g$
			1557					
					1522			
					1506			
$2a_g$	1552	1465	1517	1485*				
$3a_g$	1494	1427	1492	1441*				
					1440*	1454	1391	$4a_g$
			1416	1414				
					1388			
					1366*			
$5a_g$	1285	1287	1311	1323*				
$29b_{1u}$		1287	1282	1273				
			1258					
					1195*	1206	1196	$5a_g$
			1173	1175				
			1124	1124				
				1056				
			1011	1013				
$6a_g$	990	979	980					
					962*	1003	978	$6a_g$
			959					
			922	922				
			887	881				
					836*			$?b_{3u}$
					823*			$?b_{3u}$
$??b_{1u}$	771		770					
					721*	713	725	$7a_g$
$33b_{1u}$		672	687					
					616*	596	613	$8a_g$
$9a_g$		508	474	475				

[a]M. E. Kozlov, K. I. Pokhodnia and A. A. Yurchenko, *Spectrochim. Acta*, 1987, **43**, 323. [b]R. Swietlik, C. Garrigou-Lagrange, C. Sourisseau, G. Pages and P. Delhaes, *J. Mater. Chem.*, 1992, **2**, 857. [c]T. Takenaka, *Spectrochim. Acta*, 1971, **37**, 1535. [d]R. Bozio, I. Zanon, A. Girlando and C. Pecile, *J. Chem. Soc., Faraday Trans.*, 1978, **74**, 235.

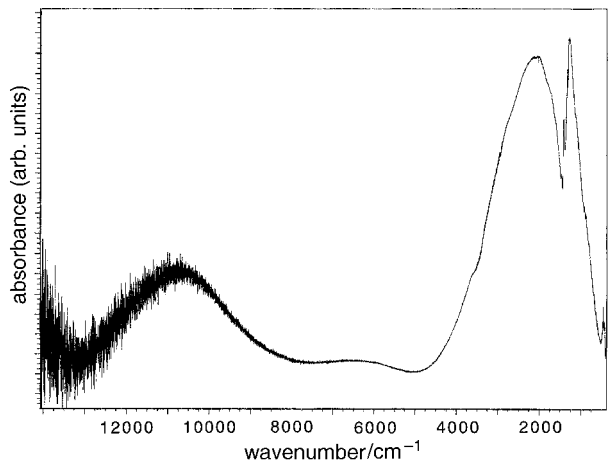

Fig. 4 Absorption spectra of **2**(PF_6) in KBr pellet at room temperature

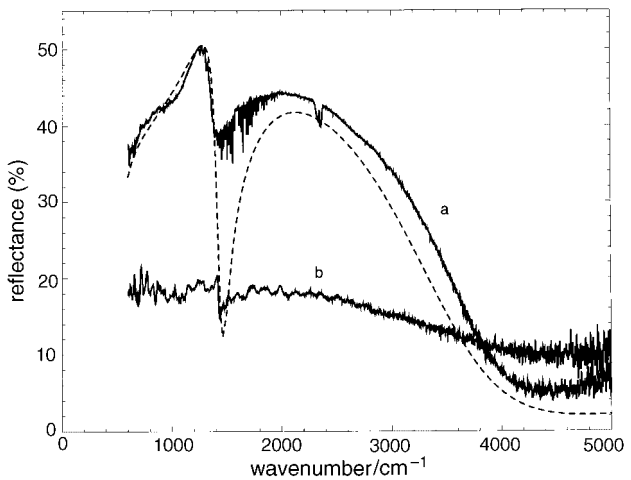

Fig. 5 Room-temperature reflectance of a **2**(BF_4) single crystal in polarization parallel (a) and perpendicular (b) to the needle axis, and theoretical calculations (dotted line)

This fit confirms that **2** does not play any role in the charge-transfer processes.

Magnetic properties

The compounds have been studied by EPR on single crystals in a Bruker ESP 300 E apparatus, equipped with an Oxford liquid-helium temperature accessory, in the temperature range 3.2–300 K. The bulk dc susceptibility and the field dependence of the magnetization have been measured in a SQUID magnetometer (Quantum MPMS-5), in the temperature range 1.7–300 K, with a magnetic field strength up to 50 kG (5 T).

At room temperature we have measured the angular dependences of the EPR *g*-factor and the peak-to-peak linewidth (ΔH) for both salts and calculated χ_s, the spin susceptibility, in comparison with a stable free radical, diphenylpicryl hydrazyl (DPPH) as reference.

The *g*-factor and the linewidth values exhibit classical anisotropy, fitting a cosine square law, which allowed us to determine the principal components (Table 4).

Two essential observations are found from these room-temperature experiments. (i) The relaxation mechanisms and therefore the linewidth values are a function of the electronic

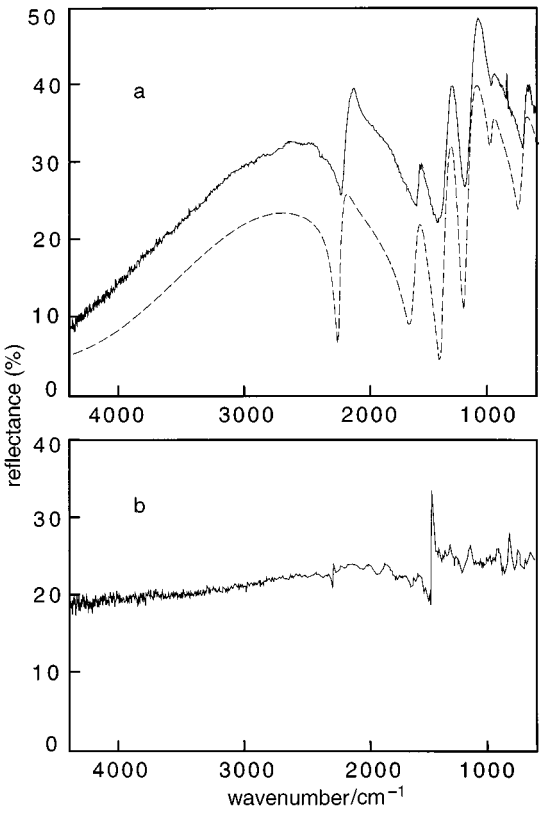

Fig. 6 Room-temperature reflectance of a **2**$(TCNQ)_3$ single crystal in polarization parallel (a) and perpendicular (b) to the needle axis, and theoretical calculations (dotted line). The reflectance has been calculated for two electrons per trimer model with $\omega_{CT}=2500\ cm^{-1}$, $\Gamma=2200\ cm^{-1}$, $M=0.78$, $R=3.4$ A, $V=1736\ A^3$, $e_\infty=3$ and seven intramolecular vibrations at $\omega_\alpha=2210$, 1630, 1395, 1180, 958, 718 and 567 cm^{-1}, $g_\alpha=350$, 540, 500, 300, 85, 190 and 50 cm^{-1}, respectively.

Table 4 Room-temperature EPR characteristics for the two charge-transfer salts

	$(D-\sigma-D)(BF_4)$	$(D-\sigma-D)(TCNQ)_3$
g_{min}	2.0011	2.0023
g_{int}	2.0044	2.0047
g_{max}	2.0084	2.0090
ΔH_{min}	66.0	1.43
ΔH_{int}	68.6	1.95
ΔH_{max}	71.4	2.25
$\chi_{s(300)}$	9.7×10^{-5}	3.3×10^{-3}

dimensionality.[5] In a quasi-one-dimensional electronic system the linewidths are narrower than in a two-dimensional one, in general being about an order of magnitude less. Therefore it seems that the TCNQ complex behaves as a quasi-one-dimensional system with a preferential stacking direction. The BF_4 salt shows a broad signal, with a ΔH value close to those of κ-phase materials, which are lamellar-like.

(ii) *g*-Factor values are molecular characteristics more or less constant for a given radical ion. For instance, the mean *g*-value $\overline{g_{RT}}=2.0072$ for $TTF^{\cdot+}$ and 2.0063 for $BEDT^{\cdot+}$.[5] For **2**(BF_4) $\overline{g_{RT}}=2.0046$, a rather low value which could arise from the large molecular size and a smaller spin–orbit coupling interaction. For the TCNQ complex we find a rather similar value, $\overline{g_{RT}}=2.0053$. This EPR signal is attributed to an exchange narrowing effect commonly observed in charge-transfer compounds such as TTF-TCNQ.[18] In such a case the averaged *g*-factor is given as:

$$\bar{g}=(g_D\gamma_D+g_Q\chi_Q)/(\chi_D+\chi_Q) \quad (4)$$

Here D corresponds to the radical donor and Q to the $TCNQ^-$ ($\overline{g_Q}=2.0026$). In this case, $(D-\sigma-D)^{2+}$ is considered as a pair of radical cations, similar to $BEDT^{\cdot+}$. If we assume the same *g*-factor we can estimate that less than one quarter of the spin susceptibility is due to the TCNQ entities.

Another important point is that the maximum *g*-factor is not in the same direction for the two types of salt. For the BF_4 salt, the maximum is found when the long axis of the crystal is parallel to the magnetic field. However for the TCNQ salt the long axis is perpendicular to the field. That indicates that the structural organisation of the donor molecules is very different in both compounds.

Temperature dependence for the BF_4 salt. The EPR temperature variation of this salt shows some similiarity in behaviour with $(EDT-DMT-TTF)_2PF_6$, $\mathbf{1}_2PF_6$, which shows a constant decrease in χ_S with temperature, and decreases to 40% of its room temperature value.[19] This is similar to the thermal behaviour of **2**(BF_4) at temperatures >100 K [Fig. 7(a)]. At 100 K, however, there is an abrupt change in the slope of the spin susceptibility, which almost disappears at *ca.* 50 K. We propose that the EPR signal below 50 K is a Curie tail corresponding to a small fraction of localized spins.

However, the variation of the linewidth, ΔH, [Fig. 7(b)] is smooth, with no sudden variation. This type of transition, with a sharp variation in χ_S but a constant decrease of ΔH, has been observed in some phases of $(BEDT)_4[M(CN)_4]$ (M = Ni, Pt)[20,21] where the electrical charge in the BEDT moiety is the same as in our compound ($\rho=1/2$). The increase in the value of the *g*-factor is associated with the localization of the charge on the donors, approaching that of the isolated radical cation.

The behaviour is reminiscent of a spin Peierls type transition, posibly associated with a large fluctuation regime. In the absence of low-temperature structural information, we assume

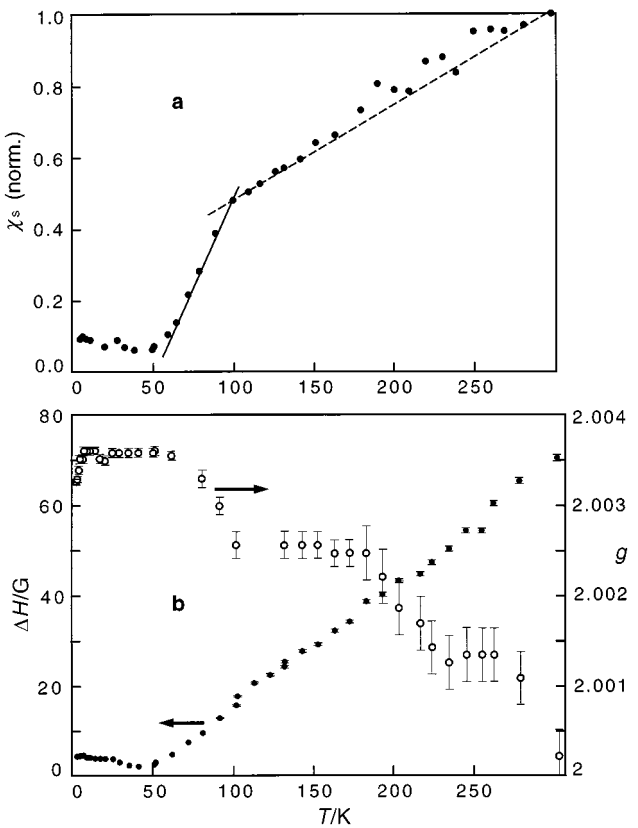

Fig. 7 (a) Temperature dependence of the normalized spin susceptibility for a **2**(BF_4) single crystal. (b) Linewidth and *g*-factor temperature dependences corresponding to their minimum values for a **2**(BF_4) single crystal.

that when the temperature is lowered the salt evolves from $(D–\sigma–D)^{\cdot+}{}_2(BF_4^-)_2$ to $(D–\sigma–D)^{2+}(D–\sigma–D)^0(BF_4^-)_2$. This hypothesis rationalizes the change of the *g*-factor towards the value for $BEDT^{\cdot+}$ at very low temperature.

Temperature dependence for the TCNQ complex. The *g*-factor shows an increase with a decrease in temperature, and reaches the value for the isolated $BEDT^{\cdot+}$ radical cation (Fig. 8).This shows that only the donor moiety is responsible for the magnetic characteristics at low temperatures, and that the contribution of $TCNQ^{\cdot-}$ becomes negligible. The linewidth however shows a more notable phenomenon, with a clear maximum at low temperature, corresponding also to a weak maximum in the *g*-factor. Generally these effects are related to the onset of an internal magnetic field owing to the appearance of magnetic fluctuations. The EPR spin susceptibility shows a Curie–Weiss behaviour with a Weiss constant ($\theta = 5$ K) characteristic of antiferromagnetic interactions.

The bulk magnetism, as measured in a SQUID magnetometer, confirms these results and gives more information. A plot of χT *vs.* *T* after diamagnetic core corrections is shown in Fig. 9. The temperature dependence can be divided into two regimes.

At rather high temperature a Curie term is still present below 150 K which corresponds to a little more than two independent electrons ($C = 0.750$). This indicates that the donor is wholly as the $(D–\sigma–D)^{2+}$ species, behaving as a biradical. Also, there is a small contribution due to the TCNQ stacks, with localized spins below the Mott–Hubbard localization (Fig. 3).

At low temperature ($T < 50$ K) a different situation arises

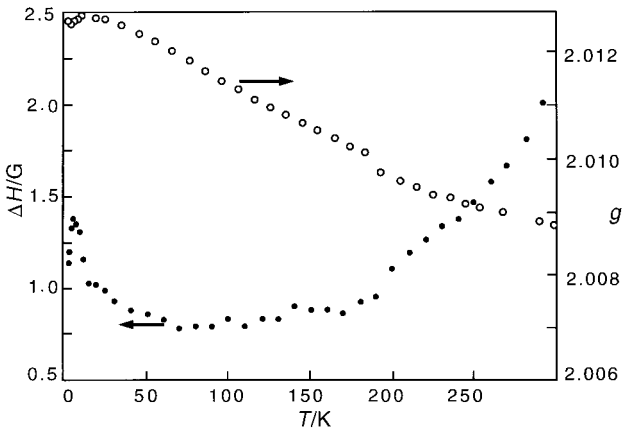

Fig. 8 Linewidth and *g*-factor temperature dependences corresponding to their maximum values for a $\mathbf{2}(TCNQ)_3$ single crystal. The error bars are small and not indicated.

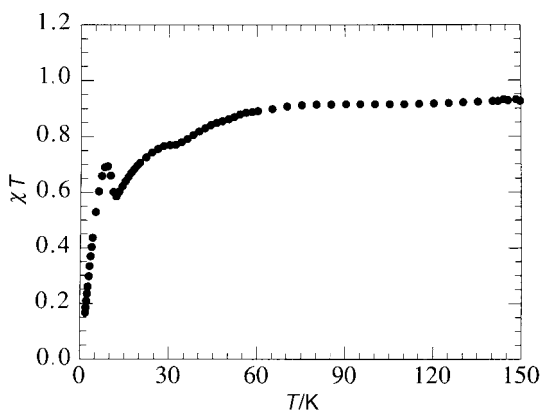

Fig. 9 Plot of χT *vs.* *T* for bulk polycrystalline $\mathbf{2}(TCNQ)_3$ between 2 and 150 K

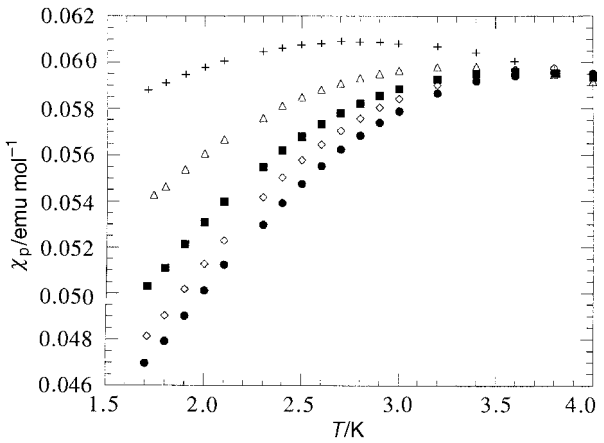

Fig. 10 Temperature and field dependences of the magnetic susceptibility for bulk polycrystalline $\mathbf{2}(TCNQ)_3$ in the range 1.7–4 K (●, 10 kG; ◇, 20 kG; ■, 30 kG; △, 40 kG; +, 50 kG)

with a maximum in χT, that corresponds with the EPR observation, and with further decrease in temperature the magnetic susceptibility diminishes quickly. This is a clear sign of a magnetic phase transition. When we measured the magnetic susceptibility at different field strengths (Fig. 10), we observe a magnetic field dependence which indicates a phase transition at $T_C \approx 4$ K. It should be remembered that for low-dimensional compounds in an insulating state, the spin ordering at low temperature can usually occur with two possible ground states;[22] an antiferromagnetic (AF) or a spin–Peierls (SP) state. In both cases the 3d ordering is due to significant interchain (or interplane) magnetic interactions with a structural change for a SP transition.

Our preliminary data are rather in favour of an AF state below 4 K but we were not able to detect any spin–flop transition up to 50 kG, contrary to what is usually observed in this class of solid. Nevertheless in the precursor regime below 50 K we have evidenced AF interactions between the bis-cation radical of **2** which should not involve the anion radical species as indicated by the *g*-factor temperature dependence (Fig. 8). This picture is clearly different from the behaviour described by Iwasa *et al.*[15] who evidenced an AF ground state for one phase of (BEDT-TTF)(TCNQ) where the TCNQ stacks are responsible for the magnetic phase transition. The picture that emerges is a charge-transfer complex with a degree of ionicity $\rho \approx 2/3$, *i.e.* $(D–\sigma–D)^{2+}(TCNQ)_3{}^{2-}$. On one hand the bis-functional donor **2** behaves as a biradical since the two TTF-type moieties are connected by an inert link and on the other hand one should expect TCNQ trimers with two electrons to be able to give rise to a singlet ground state at low temperature.

We clearly need more accurate structural information, with better crystals, to advance further explanations of the low-temperature magnetic properties. It is however possible to speculate that we have a mixed situation where the donor part takes part in AF intermolecular couplings while the supposed TCNQ stacks are involved in a transition associated with the high-temperature electronic localization observed around 250 K.

Conclusion

A bis-functional TTF type donor containing a transition metal has been synthesized and characterized. This new diamagnetic (D–σ–D) molecule is robust and shows two degenerate redox functionalities in solution. We have therefore been able to prepare new charge-transfer salts either by electrocrystallization (BF_4 salt) or by diffusion (TCNQ complex). These compounds have been thoroughly investigated and both

appear to present specific ground states. In particular, $(D–\sigma–D)(TCNQ)_3$ exhibits optical and electrical properties associated with the TCNQ moieties, whereas the low-temperature magnetic behaviour is attributed to the bis-functional donor.

This study illustrates the inter-relation between electrical and magnetic properties. It will be of interest to prepare a hybrid molecule containing a transition metal showing unpaired spins where intermolecular magnetic exchange and intramolecular charge transfer of π electrons can occur.

We thank J. Amiell (CRPP), and Drs. I. Bravic and B. Desbat (University of Bordeaux I) for their help in EPR spectroscopy, the Laue experiments and IR reflectivity measurements, respectively. J. R. acknowledges a EU fellowship associated with Network contract ERBCHRXCT930271.

References

1 M. Adam and K. Mullen, *Adv. Mater*., 1994, **6**, 439.
2 T. Otsubo, Y. Aso and K. Takimiya, *Adv. Mater*., 1996, **8**, 203.
3 Y. Misaki, H. Nishikawa, T. Yamabe, T. Mori, H. Inokuchi, H. Mori and S. Tanaka, *Chem. Lett*., 1993, 729.
4 H. Nishikawa, S. Kawauchi, Y. Misaki and T. Yamabe, *Chem. Lett*., 1996, 43.
5 J. M. Williams, J. R. Ferraro, R. J. Thorn, K. D. Carlson, U. Geisen, H. H. Wang, A. M. Kini and M.-H. Whangbo, *Organic Superconductors* (*including Fullerenes*), Prentice Hall, Englewood Cliffs, 1992.
6 A. Graja, V. M. Yartsev, C. Garrigou-Lagrange, M. Salle and A. Gorgues, *Phys. Status. Solidi* (*B*), 1992, **174**, 119.
7 H. Tajima, M. Arifuku, T. Ohta, T. Mori, Y. Misaki, T. Yamabe, H. Mori and S. Tanaka, *Synth. Met*., 1995, **71**, 1951.
8 A. Graja, A. Lapinski, M. Salle and A. Gorgues, *Synth. Met*., 1995, **67**, 1903.
9 X. Gan, M. Munataka, T. Kuroda-Sawa and M. Maekawa, *Bull. Chem. Soc. Jpn*., 1994, **67**, 3009.
10 M. Munakata, T. Kuroda Sowa, M. Maekawa, A. Hirota and S. Kitagawa, *Inorg. Chem*., 1995, **34**, 2705.
11 R. D. McCullough and J. A. Belot, *Chem. Mater*., 1994, **6**, 1396.
12 N. Le Narror, N. Robertson, E. Wallace, J. D. Kilburn, A. E. Underhill, P. N. Bartllett and N. Webster, *J. Chem. Soc., Dalton Trans*., 1996, 823.
13 N. Sventrup and J. Becher, *Synthesis*, 1995, 215.
14 P. Frere, R. Carlier, K. Boubekeur, A. Gorgues, J. Roncali, A. Tallec, M. Jubault and P. Batail, *J. Chem. Soc., Chem. Commun*., 1994, 2071.
15 Y. Iwasa, K. Mizuhashi, K. Toda, Y. Tokura and G. Saito, *Phys. Rev. B*, 1994, **49**, 3580.
16 M. J. Rice, *Solid State Commun*., 1979, **31**, 93; M. J. Rice, V. M. Yarsev and C. S. Jacobsen, *Phys. Rev. B*, 1980, **21**, 3437.
17 V. M. Yartsev, *Phys. Status Solidi* (*B*), 1982, **112**, 279.
18 Y. Tomkiewicz, A. R. Taranko and E. M. Engler, *Phys. Rev. Lett*., 1976, **37**, 1705.
19 A. Otsuka, G. Saito, T. Sugano, M. Kinoshita and K. Honda, *Thin Solid Films*, 1989, **179**, 259.
20 M. Tanaka, H. Takeuchi, M. Sano, T. Enoki, K. Suzuki and K. Imaeda, *Bull. Chem. Soc. Jpn*., 1989, **62**, 1432.
21 C. Garrigou-Lagrange, J. Amiell, E. Dupart, P. Delhaes, L. Ouahab, M. Fettouhi, S. Triki and D. Grandjean, *Synth. Met*., 1991, **41–43**, 2053.
22 C. Coulon, in *Organic and inorganic Low-dimensional Crystalline Materials*, ed. P. Delhaes and M. Drillon, NATO AISI series 1987, vol. 168B, p. 201.

Paper 6/08575J; *Received* 23*rd December*, 1996